AEROSPACE REPORT NO.
TR-2007(8555)-1

Stroboscopic Imaging Interferometer for MEMS Performance Measurement

15 July 2007

Prepared by

J. A. CONWAY and J. V. OSBORN
Electronics and Photonics Laboratory
Laboratory Operations

J. D. FOWLER
Aerospace Engineering Department
University of California, Los Angeles, 90095

Prepared for

SPACE AND MISSILE SYSTEMS CENTER
AIR FORCE SPACE COMMAND
483 N. Aviation Blvd.
El Segundo, CA 90245-2808

Engineering and Technology Group

THE AEROSPACE CORPORATION
El Segundo, California

This report was submitted by The Aerospace Corporation, El Segundo, CA 90245-4691, under Contract No. FA8802-04-C-0001 with the Space and Missile Systems Center, 483 N. Aviation Blvd., El Segundo, CA 90245. It was reviewed and approved for The Aerospace Corporation by B. Jaduszliwer, Principal Director, Electronics and Photonics Laboratory; and D. C. Marvin, Principal Director, Research and Program Development Office. Michael Zambrana was the project officer for the Mission-Oriented Investigation and Experimentation (MOIE) program.

This report has been reviewed by the Public Affairs Office (PAS) and is releasable to the National Technical Information Service (NTIS). At NTIS, it will be available to the general public, including foreign nationals.

This technical report has been reviewed and is approved for publication. Publication of this report does not constitute Air Force approval of the report's findings or conclusions. It is published only for the exchange and stimulation of ideas.

Michael Zambrana
SMC/EA

REPORT DOCUMENTATION PAGE

Form Approved
OMB No. 0704-0188

1. REPORT DATE (*DD-MM-YYYY*)	2. REPORT TYPE	3. DATES COVERED *(From - To)*
15-07-2007		

4. TITLE AND SUBTITLE

Stroboscopic Imaging Interferometer for MEMS Performance Measurement

5a. CONTRACT NUMBER
FA8802-04-C-0001

5b. GRANT NUMBER

5c. PROGRAM ELEMENT NUMBER

6. AUTHOR(S)

J. A. Conway, J. V. Osborn, and J. D. Fowler

5d. PROJECT NUMBER

5e. TASK NUMBER

5f. WORK UNIT NUMBER

7. PERFORMING ORGANIZATION NAME(S) AND ADDRESS(ES)

The Aerospace Corporation
Laboratory Operations
El Segundo, CA 90245-4691

8. PERFORMING ORGANIZATION REPORT NUMBER

TR-2007(8555)-1

9. SPONSORING / MONITORING AGENCY NAME(S) AND ADDRESS(ES)

Space and Missile Systems Center
Air Force Space Command
483 N. Aviation Blvd.
El Segundo, CA 90245

10. SPONSOR/MONITOR'S ACRONYM(S)
SMC

11. SPONSOR/MONITOR'S REPORT NUMBER(S)

12. DISTRIBUTION/AVAILABILITY STATEMENT

Approved for public release; distribution unlimited.

13. SUPPLEMENTARY NOTES

14. ABSTRACT

The insertion of MEMS components into aerospace systems requires advanced testing to characterize performance in a space environment. Here we report a novel stroboscopic interferometer test system that measures nanometer-scale displacements of moving MEMS devices. By combining video imagery and phase-shift interferometry with an environmental chamber, rapid visualization of the dynamic device motion under the actual operational conditions can be measured. The utility of this system is further enhanced by integrating the interferometer onto the chamber window, allowing for robust interferometric testing in a noisy environment without requiring a floating optical table. To demonstrate these unique capabilities, we present the time-resolved images of an electrostatically actuated MEMS cantilevered beam showing the first- through sixth-order plate modes under vacuum.

15. SUBJECT TERMS
Microelectromechanical devices, MEMS metrology, stroboscopic interferometer system, vacuum systems, interferometry

16. SECURITY CLASSIFICATION OF:			17. LIMITATION OF ABSTRACT	18. NUMBER OF PAGES	19a. NAME OF RESPONSIBLE PERSON
a. REPORT	b. ABSTRACT	c. THIS PAGE			Josh Conway
UNCLASSIFIED	UNCLASSIFIED	UNCLASSIFIED		17	19b. TELEPHONE NUMBER *(include area code)* (310)336-5146

Contents

Figures

Tables

1. Introduction

The harsh environments and stringent reliability requirements of aerospace systems demand detailed knowledge of the motion of all mechanical and electro-mechanical devices.[1] The functional performance must be well understood, and the failure modes catalogued. While this may entail a straightforward analysis for macroscopic devices, microscopic electro-mechanical structures require new tools to study their response under various conditions. In the existing art, static, quasi-static, and vibrometer-based[2,3] methods are employed, and the motion of Micro-Electro-Mechanical Systems (MEMS) is then analytically reconstructed. These inferential results can be unacceptable for the requirements of modern aerospace applications. For instance, quasi-static measurements are often lacking in precision when related to dynamic operation, especially near a mechanical resonance. Vibrometer-based measurements, on the other hand, provide tremendous precision for dynamic measurement, but are not able to yield a complete picture of the device motion. While vibrometry is able to map amplitude and phase of vibration across a surface, it cannot yield static topographic information.

Direct measurement of moving parts makes new demands on the test system. To study the motion of microscopic mechanical parts, one cannot simply attach sensors, and non-contact measurement techniques are required. Further complicating the measurement process are the environments in which MEMS operate. The characterization of MEMS devices for terrestrial applications typically must be performed at partial pressures of gas and over a range of temperatures to replicate packaged environments and to optimize their performance. Emerging applications of MEMS in space systems, however, require functionality under extreme environmental conditions. Such applications include spatial light modulation on the cryogenic focal plane of imaging systems,[4] switching and phase modulation for massively parallel phased arrays,[5] and thermal control directly on the skin of surfaces.[6] In these situations, packaging may be minimal, temperature ranges extreme, and pressure as low as the vacuum of space. The testing conditions must therefore match the operational environment for MEMS technology to establish itself in this market.

In response to these challenges, various test systems have been reported in the literature. There are those specifically designed for space applications that recreate the temperatures and pressures of the space environment, but employ probe or scanning techniques that do not give a complete picture of the device dynamics or topology. [1,7] In contrast, optical stroboscopic MEMS test systems have been reported[8–12] that characterize devices in motion. These yield a complete picture of the dynamic motion and surface structure of the device down to the nanometer scale, but those reported in the literature only operate under ambient conditions. Neither of these classes of test systems can make dynamic measurements while simulating the pressures encountered in space and the upper atmosphere. This is a critical point because MEMS dynamic response changes markedly when the damping of atmospheric pressure is removed, especially near mechanical resonant frequencies.[13–17]

Addressing these issues, our solution is based on a fusion of these designs. By integrating an environmental test chamber with a stroboscopic imaging interferometer, we have created a system capable of generating a complete picture of the device dynamics with variable environmental control. This

combination of techniques, however, goes further than simply adding new environmental controls to standard stroboscopic phase-shift interferometry. In fact, the system becomes much more than the sum of its parts. Our results show that the integration of the interferometer directly onto the environmental chamber greatly reduces the measurement errors incurred from external vibrations, which has limited the utility of many interferometric measurement systems. By keeping all of the interferometer optics rigidly attached to the face-plate of the environmental chamber, deep sub-wavelength out-of-plane resolution has been achieved in a very noisy laboratory without the use of a floating optical table. This single advance has the capability of bringing interferometric MEMS characterization out of the controlled laboratory environment and onto the factory floor.

2. Optical Design

Our test system is based on the stroboscopic Michelson interferometer. It achieves nanometer-scale, out-of-plane resolution interferometrically and diffraction-limited lateral resolution (~1 μm) using microscope objectives. Although it relies on sampling measurements during cyclical motion of the device, only five intensity images are used to reconstruct each "frozen" surface per time step of motion. At standard video refresh rates of 15 Hz, this makes for rapid frame acquisition, which is robust in the face of environmental noise. Because a video camera is employed as a detector array, no lateral scanning is required. This popular optical design has been reported in the literature,[18] and our instrument design evolved out the work of Muller.[8–10] In our attempt to recreate Muller's stroboscopic measurement system, we found that those designs proved too susceptible to vibrations to yield reproducible results in our noisy lab environment. Even through the use of 1.5-in. optical post assemblies, a floating optical table and heavy laser isolation curtains, noise continued to plague this system. Resolution of this problem led to several important improvements to be discussed below. Although we have machined hardware and developed software to perform the data acquisition and processing operations, the design is simple enough to be replicated in other labs, unlike white-light and more complicated interferometers.[19]

The layout for the test system is illustrated in Figure 1. The light source is a fiber-coupled diode laser operating at 635 nm (Melles Griot 57ICS062/SP/HS). This laser is directly modulated such that the beam is pulsed on and off with a programmable delay in synchrony with the MEMS driving signal. In doing so, this stroboscopic source is able to "freeze" the device at any phase of its high-speed motion, even when employing slow cameras and detectors. To keep the image from blurring with the MEMS motion, the duty cycle (defined here as the optical pulse duration/period of the MEMS driving signal) was kept below 0.01. This low duty cycle, however, has the effect of greatly reducing the optical power falling on the camera (Pulnix TM-1020). Because the out-of-plane resolution depends strongly on the number of digitized bits in the detected signal,[20] it is necessary to cover the 8-bit dynamic range of the camera. To correct for this without introducing expensive high-power lasers, focusing optics were introduced into the optical path to concentrate the beam onto the region of interest on the device. It is important to note that microscope objectives should not be used for this task.

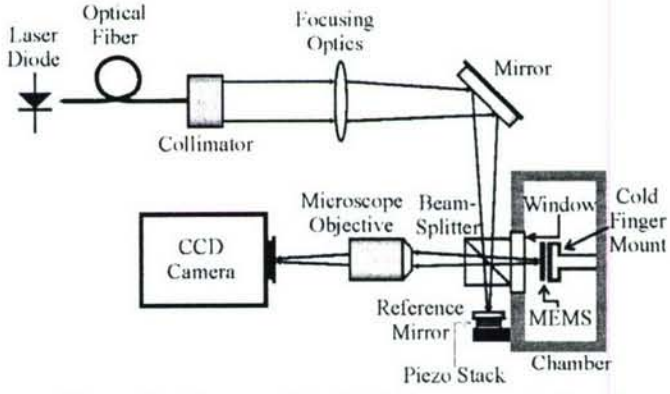

Figure 1. The optical layout of the MEMS stroboscopic interferometer.

High-numerical-aperture optics make calibration very difficult due to their rapidly changing phase front near the focus. This is because the radius of curvature of the phase must change from a very small quantity near the focus to infinity at the actual focal spot.[21] If the reference mirror and test device are not equidistant from their objective lenses, the phase fronts will have different curvatures. After unwrapping, this curvature translates into warped surface reconstructions even if the sample and reference mirror are both perfectly planar. Although the peak output power of our laser source is 7 mW, we have found that a low-magnification lens system can easily correct phase-curvature problems while concentrating enough light to saturate the charge-coupled device (CCD) camera.

After the focusing optics, the beam encounters a non-polarizing beam splitter. This sends half of the light into the environmental chamber and onto the MEMS device under test. The remaining half of the optical beam is sent to a reference mirror on a PZT (lead zirconate titanate) transducer, forming the second arm of a Michelson interferometer. These beams then recombine and interfere, allowing one to determine out-of-plane displacement. The nature of the measurement can allow for measurement sensitivity down to the nanometer scale.[19] Seen from a different perspective, though, this sensitivity makes the measurement prone to error from noise and vibration. Nanoscale displacement or vibration in any part of the optical path in either arm is translated into measurement error. The reader is reminded that the phase unwrapping process can greatly amplify these errors by incorrectly adding or subtracting multiples of $\lambda/2$. It is for precisely this reason that external noise has plagued optical interferometric measurements and why most systems only operate in highly isolated laboratory environments.

To correct for this, we have integrated the interferometer onto the faceplate of the environmental chamber. The beam splitter is fixed with optical epoxy to the chamber window, and the reference mirror is bolted directly to the common chamber faceplate. Because the interferometer measures relative displacement between the two arms, the measurement is exceedingly sensitive to noise in this region. To correct for this, the optical path of each arm was kept shorter than 2 cm. These simple design changes had a profound effect on the performance of the interferometer. Although the majority of the data reported in this report was taken on a floating optical table, it was later found that the performance was not significantly degraded when the table was not floating. In addition to this, the system was able to take data with nanometer-scale out-of plane resolution in an exceptionally noisy environment and while the chamber was rigidly attached to an operating roughing pump and turbo pump. Unlike the holographic techniques or the use of specialized interferometers,[11] our design achieves this high stability without the use of custom components. The power of this architecture is that it can be assembled from common laboratory equipment.

After the beams recombine at the beam-splitter, a long-working-distance objective is used to image the device onto a CCD camera. This system takes an entire image at once, so no lateral scanning is required. The captured image is covered with fringes, as shown in Figure 2(b). To obtain the actual phase data from the fringe pattern, we used phase-shift interferometry.[18] This entails translating the reference mirror longitudinally by a fixed displacement between each frame. Of the various recipes for this, we employed Hariharan's algorithm,[22] which uses intensity data at five known positions of the reference mirror to generate phase data. This yields the relative phase modulo 2π. Converting this wrapped phase to absolute phase in two dimensions is still considered an unsolved problem in the field.[23] To unwrap the phase over its full range, we used the method of Volkov and Zhu.[24] The absolute phase (denoted by ψ) is calculated using Eq. (1).

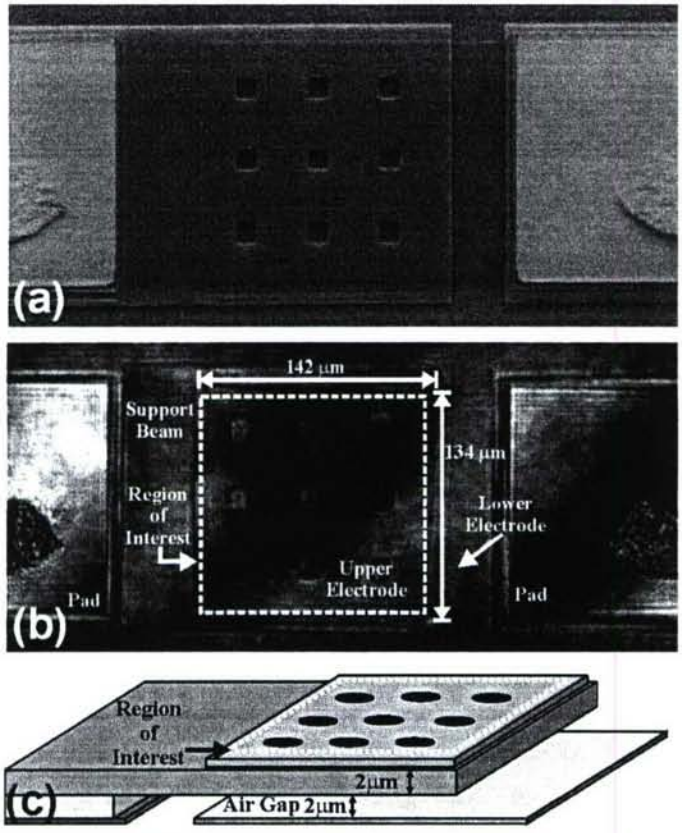

Figure 2. MEMS cantilever device. (a) Imaged by a scanning electron microscope (SEM), and (b) imaged directly in interferometer system showing a fringe pattern. (c) Graphical rendering of the cantilever beam illustrating the profile.

$$\psi = \mathrm{Re}\left\{\frac{1}{2\pi i}F^{-1}\left[\frac{F(\partial_x\psi)q_x + F(\partial_y\psi)q_y}{q_x^{\,2} + q_y^{\,2}}\right]\right\} \quad (1)$$

F and F^{-1} represent Fourier and inverse Fourier transforms, respectively, and q represents the wave vector in a given direction. Equation (1) requires the gradient of the absolute phase, which can be calculated directly from the wrapped phase[25] using Eq. (2).

$$\begin{aligned}\partial_x\psi(x,y) = &-\sin\psi(x,y)*\left[\cos\psi(x+dx,y)-\cos\psi(x,y)\right]\\ &+\cos(x,y)*\left[\sin\psi(x+dx,y)-\sin\psi(x,y)\right]\end{aligned} \quad (2)$$

The gradient in the *y*-direction is determined in a similar manner by permuting the *x* and *y* dimensions in Eq. (2). Combining the two equations above yields an initial value for the absolute phase. From Eq. (1), it can be seen that the DC term of the Fourier expansion must be dropped ($q_{x=0} = q_{y=0} = 0$)

because of the resultant null in the denominator. To resolve this ambiguity, the wrapped phase is then subtracted from this unwrapped phase, and the resultant difference is rounded to the nearest 2π. The wrapped phase is added back, and the absolute phase is obtained.

3. Results

To demonstrate the capabilities of this MEMS Stroboscopic Interferometer, we have examined the motion of a MEMS cantilever beam test structure. The sample device comprises two electrical bond pads connected to two doped, 150 x 150 μm overlapping polysilicon layers, with an isolating 2-μm air-gap, supported by a 134 x 30 μm polysilicon beam, also shown in Figure 2. The holes in the paddle, which are designed to aid in MEMS oxide release, are also evident. Under electrical bias, electro-static deflection downwards of the upper 2-μm-thick cantilevered polysilicon region of interest occurs. A sinusoidal electric drive signal results in a cyclical device motion proportional to drive signal amplitude and in-phase with the driving waveform. This device was chosen for analysis because flexible polysilicon beam structures of this type are very common in MEMS radio-frequency switches, rate sensors, accelerometers, and many other MEMS devices.

For a given frequency, drive voltage, and chamber pressure, the MEMS Stroboscopic Interferometer can generate a surface reconstruction of the cantilever at various "frozen" phases of its motion. This is illustrated in Figures 3 and 4, which show the first and second set of three resonant modes of the

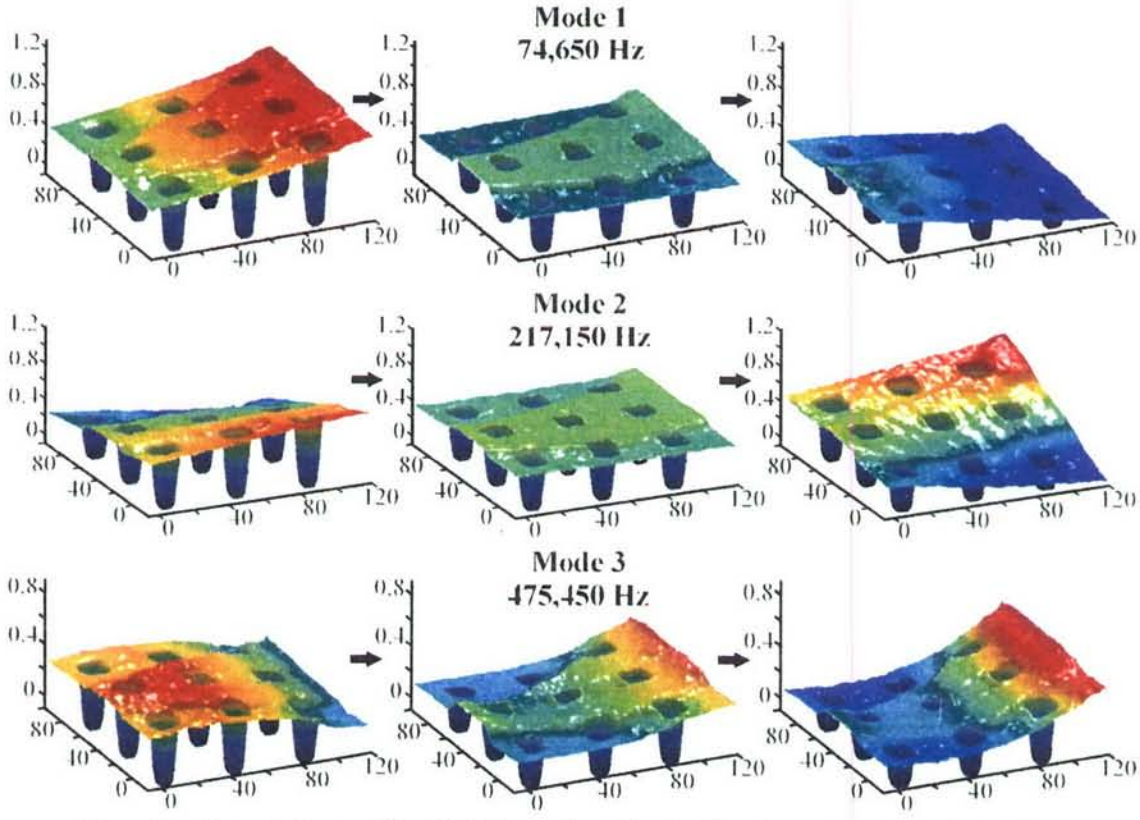

Figure 3. Several phases of the MEMS cantilever for the first three resonant modes. All units are in microns.

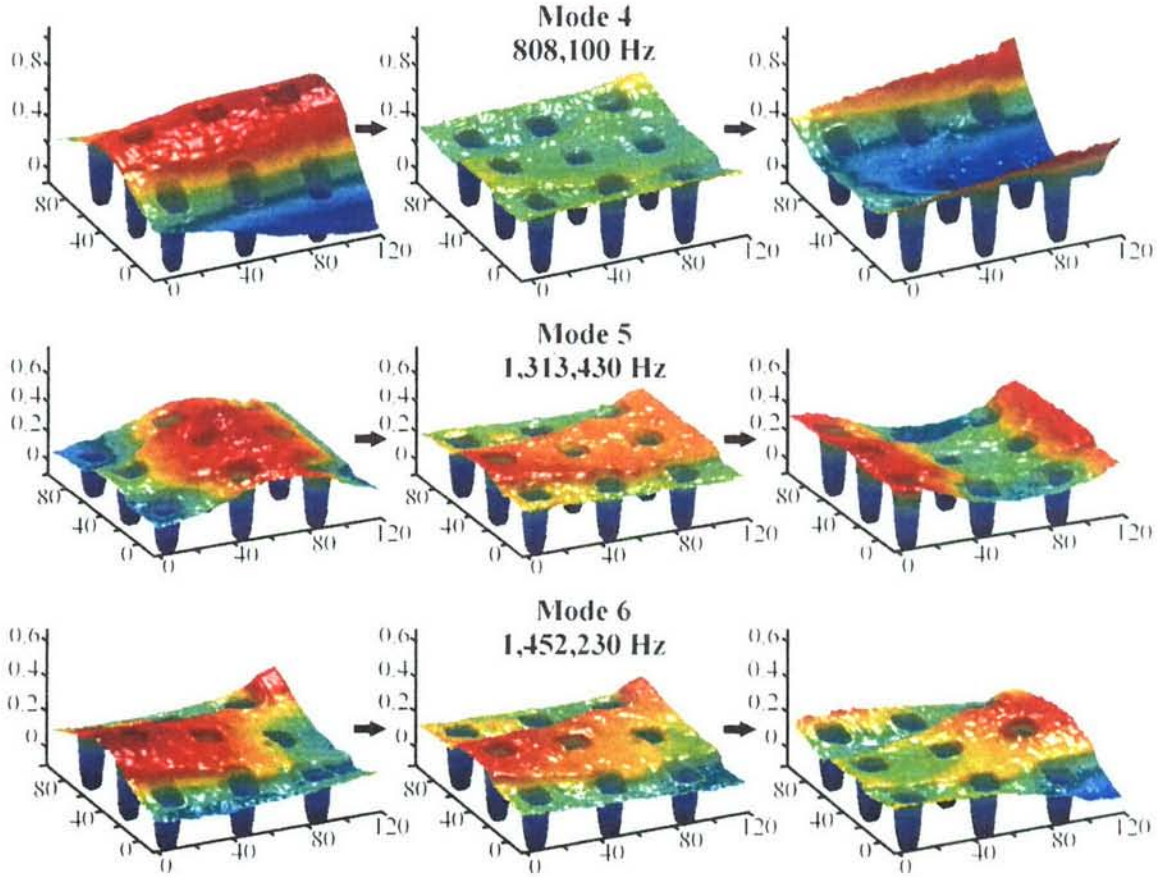

Figure 4. Several phases of the MEMS cantilever for the second three resonant modes. All units are in micrometers.

device at 10 mTorr operating pressure. These resonant modes were stimulated with sinusoidal drive signals at 74,640 Hz, 217,150 Hz, 475,450 Hz, 880,100 Hz, 1,313,430 Hz, and 1,452,230 Hz, respectively. This is the first time plate modes on this scale have been directly imaged[26] as known to the authors. Because the Quality Factor (Q-factor) varies between modes, the amplitude of the drive signal was changed to give a clear picture of device motion. The deformation of the cantilever can be clearly seen in all sets of surface reconstructions. Also evident from the surface reconstructions is the ridge across the center of the device. This artifact of fabrication is approximately 10 nm high and is very clear from this measurement.

In order to verify that we have correctly identified each of the first six resonant modes of the cantilever test structure, we have performed Finite Element Modeling (FEM) of the complete 3-D device structure. This modeling was performed using FEMLab Multiphysics software from COMSOL Inc.[27] This mechanical 3-D model is constructed from the original mask files of the cantilever device. We have used the COMSOL materials property database library values for polysilicon. When running the model, a Young's Modulus of 130 GPa was chosen such that the device resonance at the second eigenfrequency most closely matched that of the stroboscopic measurement. This is in agreement with empirically derived values of polysilicon, which have been measured between 132 and 174

Gpa.[28] All other material properties were set to their default values. The COMSOL eigenfrequency 3-D Solid, Stress-Strain solver was selected, with boundary conditions set such that all stationary surfaces were fixed. The first six eigenmodes are shown in Figure 5. These modeled results are in good agreement with both our measured frequencies and mode shapes. Table 1 shows the values of measured and modeled results, all with errors less than ±5%.

The strength of the resonant mechanical modes is also a critical parameter for these devices. To quantify this, we measured the mechanical response to a sinusoidal drive voltage. Cantilever devices of this type have a non-linear quasi-static response to the driving signal and "pull-in" toward the lower electrode at a given threshold voltage.[29] To minimize this effect, the amplitude of the drive voltage was changed at each pressure to keep the peak displacement below 2 μm at resonance. The motion of a small region near the free edge of the cantilever is illustrated in Figure 6(a). Due to device destruction during temperature cycling, a different MEMS device was used for these tests. This device is identical to that of Figure 2 except the single 134 x 30 μm polysilicon beam is replaced

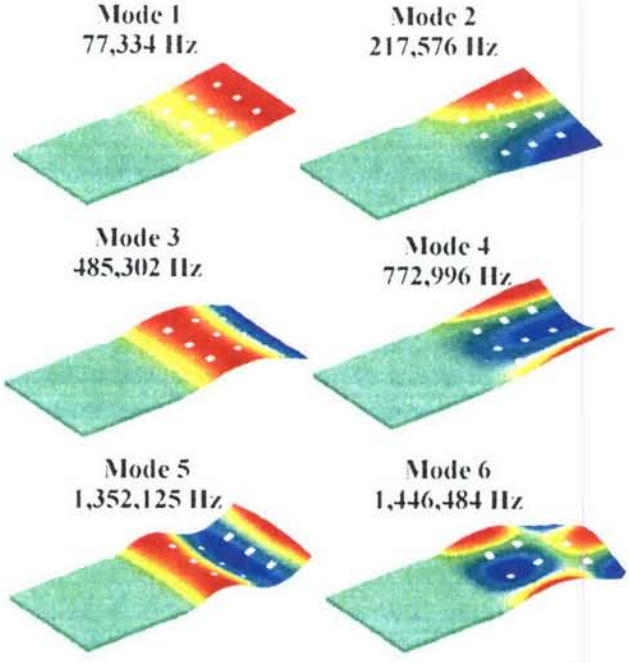

Figure 5. COMSOL 3-D Finite Element Modeled results of the MEMS cantilevered test structure. Eigenfrequencies and mode shapes of the first six resonant modes are shown.

Table 1. The eigenfrequencies for measured and modeled modes using COMSOL Multiphysics 3-D FEM, Solid, Stress-Strain Solver.

Mode ID	Measured (kHz)	Modeled (kHz)	% Delta
Mode-1	74.65	77.33	-3.6%
Mode-2	217.15	217.576	-0.2%
Mode-3	475.45	485.302	-2.1%
Mode-4	808.1	772.996	4.3%
Mode-5	1,313.43	1,352.13	-2.9%
Mode-6	1,452.23	1,446.48	0.4%

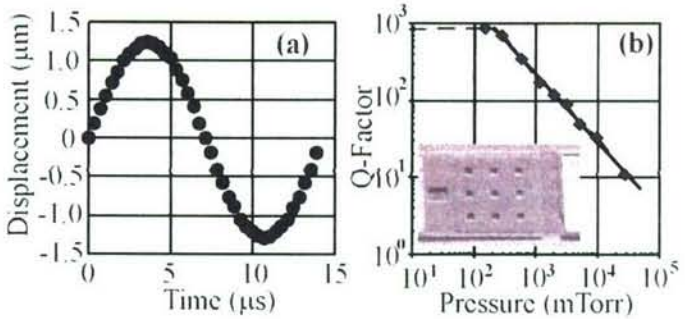

Figure 6. Cantilever motion and Q-factor. (a) The displacement of a single point on the cantilever at the fundamental resonance (70,040Hz). (b) The Q-factor of the fundamental mode over pressure. The inset shows an SEM image of the cantilever under test.

by a pair of 64 x 30 μm beams, as shown in the inset of Figure 6(b). The mechanical response was then recorded about the first resonance peak, and the Q-factor was computed from the central frequency divided by the spectral Full-Width at Half Maximum (FWHM) of the mechanical displacement amplitude. The Q-factor for the fundamental mode at several pressures is plotted in Figure 6(b). This plot illustrates not only the transition to intrinsic damping near 10 mTorr but also underscores the critical importance of the environmental chamber. At atmospheric pressures, this mode is heavily over-damped, and would be very difficult, if not impossible, to study quantitatively. Thus, we see that without the combination of vacuum pressures, nano-scale sensitivity, and high-speed measurement, the complete motion of the 3-D modes of Figures 3 and 4 could not be studied.

The authors know of no reported measurement system employing a single measurement that is capable of this metrology. There are reports of vibrometer test systems with vacuum chambers,[30] but these systems cannot image surface topology directly[9] and place a great deal of strain on the scanning mechanism. It is non-trivial to translate the focusing optics or the MEMS device inside a vacuum chamber, although a confocal solution has been implemented. Digital holographic solutions, such as the Lyncée Tec DHM R1000, can provide a tool capable of measuring mechanical transients, in contrast to the repeated motion required here. Unfortunately, this system is limited to drive frequencies below 100 kHz, and therefore cannot reproduce the modes in Figures 3 and 4. White-light interferometry systems, such as the Wyko DMEMS, which can strobe up to 1 MHz,[31] suffer from similar high-frequency limitations. This is not to preclude the possibility of altering the test equipment to achieve higher frequency operation,[32] employing a system that uses a combination of white-light interferometry and vibrometry, such as the Polytec MSA-400, or a system of white-light and phase-shift interferometry, such as Micro Photonics Zoomsurf 3D. We stress that although we know of no reported system that has all of the capabilities required to measure these plate modes, one could be built from competing technologies. The novelty and power of this system are in its simplicity, ease of operation, accessibility to the researcher, and noise immunity implicit in the design. Unlike packaged measurement systems, changing out the parts to add new capabilities is simple. For instance, the maximum device frequency that can be measured is determined by the laser modulation bandwidth. Telecom lasers with modulated bandwidths greater than 1 GHz are now widely available, and can be added to this system.

To quantify the vertical (interferometric) resolution in the presence of noise in real system operation, we undertook a statistical analysis. For this study, we acquired 200 phase-unwrapped surfaces of the static cantilever device over the course of 10 min. This timescale is longer than the typical measurement, but was needed to achieve a large statistical sample. It was seen that the device as a whole drifted on the order of 10 nm during the experiment. To compensate for this, the motion of the substrate was calculated and then subtracted from that of the cantilever. After removing the drift, the standard deviation of out-of-plane position was calculated at 4224 individual points on the cantilever from these 200 surface reconstructions. The median standard deviation was calculated to be 2 nm, a surprisingly small result in a very noisy laboratory. Most of this noise can be attributed to the camera itself since we used an uncooled CCD that demonstrated an RMS dark noise of approximately 11.2 out of the full-scale 255 (8 bits) when there was no illumination. Monte Carlo simulations using a Gaussian fit to this noise showed that the camera added approximately 1.5 nm of out-of-plane uncertainty to our measurement. This large noise source can be rectified by either upgrading to a scientific-grade low-noise camera, or by averaging several datasets. The reader is also reminded, however, that these pixels represent an area of approximately 1 μm^2. For any real material, there will be a height variation across the pixel of much larger than 2 nm. For instance, 2 nm across the pixel represents a perfectly planar surface that is tilted by 0.1146° from the normal, or a perfectly oriented surface with 2 nm of root-mean-square roughness.

4. Conclusion

We have demonstrated the design and functionality of a novel stroboscopic imaging interferometer for MEMS metrology. The nano-scale precision and high-frequency capabilities make this an ideal MEMS characterization tool for devices that can be electrically actuated. By making the environmental chamber an integral part of the measurement system, we have ruggedized our optical interferometric instrument. The interferometer can function in noisy environments, greatly extending the utility of this high-precision technique.

The combined attributes of our system enable the direct observation and measurement of large area (~500 μm x 500 μm) complex 3-D motions and high-order 3-D plate modes of MEMS devices dynamically operating at frequencies in excess of 1.4 MHz. Many MEMS applications, such as spatial light modulators, inertial rate sensors, and accelerometers, demonstrate performance that lacks with respect to their macroscopic counterparts. Measurement capability such as ours can provide critical mechanical MEMS metrology well in excess of first-, second-, or third-order modal analysis. These measurement data provide the MEMS designer directly observable measurements of deformations due to high-order modes and allow proper error attribution to their sources.

Our novel tool was used to image many of the resonant modes of a cantilevered beam structure. The mechanical 3-D bending modes observed in this MEMS device, while well known in structural mechanics of large objects, are very difficult to directly measure for micron-scale MEMS devices. Direct observation, measurement, and surface reconstruction of MEMS devices while under full dynamic operation provides a unique metrology capability for understanding and observing the complex behavior of micromechanical structures.

References

1. D. J. McComas, G. P. Miller, J. N. Mitchell, S. E. Pope ,and P. W. Valek, "Space applications of microelectromechanical systems: Southwest Research Institute- vacuum microprobe facility and initial vacuum test results," *Review of Scientific Instruments*, **74**(8), pp. 3874-3878, 2003.

2. J. S. Burdess, A. J. Harris, D. Wood, R. J. Pitcher, and D. Glennie, "A system for the dynamic characterization of microstructures," *Journal of Microelectromechanical Systems*, **6**(4), pp. 322-328, 1997.

3. J. La, J. Choi, S. Wang, K. Kim, and K. Park, "Continuous scanning laser Doppler vibrometer for mode shape analysis," *Optical Engineering*, **42**, pp. 730-737, 2003.

4. H. C. Ford, M. Clampin, G. D. Illingworth, J. E. Krist, S. S. Oliver, L. Petro, and G. E. Sommagren, "Requirements for an optical 8-m space telescope with a MEMs deformable mirror to detect Earth-like planets around nearby stars," *Proceedings of SPIE*, **4854**, pp. 554-557, 2003.

5. K. J. Vinoy, V. K. Varadan, "Design of reconfigurable fractal antennas and RF-MEMS for space-based systems," *Smart Material Structures*, **10**, pp. 1211-1223, 2001.

6. R. Osiander, J. L. Champion, A. M. Darrin, J. J. Sniegowski, S. M. Rodgers, D. Douglas, and T. D. Swanson, "Micromachined louver arrays for spacecraft thermal control radiators," *Aerospace Sciences Meeting and Exhibit*, 39th, Reno, NV, Jan. 8-11, 2001.

7. B. Legrand, E. Quevy, B. Stefanelli, D. Collard, and L. Buchaillot, "Vacuum and cryogenic station for micro-electro-mechanical systems probing and testing," *Review of Scientific Instruments*, **73**(12), pp. 4393-4395, 2002.

8. M. R. Hart, R. A. Conant, K. Y. Lau, and R. S. Muller, "Stroboscopic Interferometer System for Dynamic MEMS Characterization," *Journal of Microelectromechanical Systems*, **9**(4), pp. 409-418, 2000.

9. C. Rembe, R. Kant, and R. S. Muller, "Optical measurement methods to study dynamic behavior in MEMS," *Proceedings of SPIE*, **4400**, pp. 127-137, 2001.

10. C. Rembe and R. S. Muller, "Measurement System for Full Three-Dimensional Motion Characterization of MEMS," *Journal of Microelectromechanical Systems*, **11**(5), pp. 479-488, 2002.

11. P. Hariharan, *Optical Interferometry* (Academic Press, San Diego, 2003).

12. S. Petitgrand and A. Bosseboeuf, "Simultaneous mapping of out-of-plane and in-plane vibrations of MEMS with (sub)nanometer resolution," *Journal of Micromechanics and Microengineering*, **14**, pp. S97-S101, 2004.

13. V. Mortet, R. Petersen, K. Haenen, and M. D'Olieslaeger, "Wide range pressure sensor based on a piezoelectric bimorph microcantilever," *Applied Physics Letters*, **88**(133511), 2006.

14. R. A. Buser and N. F. De Rooij, "Very high Q-factor resonators in monocrystalline silicon," *Sensors and Actuators*, **A21-A23**, pp. 323-327, 1990.

15. J. Mertens, E. Finot, T. Thundat, A. Fabre, M. Nadal, V. Eyraud, and E. Bourillot, "Distinguishing the effects of temperature, molecular adsorption, and gas properties using microcantilevers," *Ultramicroscopy*, **97**, pp. 119-126, 2003.

16. F. R. Blom, S. Bouwstra, M. Elwenspoek, and J. H. J. Fluitman, "Dependence of the quality factor of micromachined silicon beam resonators on pressure and geometry," *Journal of Vacuum Science and Technology B*, **10**, pp. 19-26, 1992.

17. K. Y. Yasumura, T. D. Stowe, E. M. Chow, T. Pfafman, T. W. Kenny, B. C. Stipe, and D. Rugar, "Quality factors in micron- and submicron-thick cantilevers," *Journal of Microelectromechanical Systems*, **9**(1), pp. 117-125, 2000.

18. W. Hemmert, M. S. Mermelstein, and D. M. Freeman, "Nanometer resolution of three-dimensional motions using video interference microscopy," *Twelfth IEEE International Conference on Micro Electro Mechanical Systems*, Orlando, FL, p. 302, 1999.

19. E. Novak, D. Wan, P. Unruh, and J. Schmit, "Dynamic MEMS measurement using a strobed interferometric system with combined coherence sensing and phase information," *Proceedings of the International Conference on MEMS, NANO and Smart Systems*, 20-23, pp. 285–288, 2003.

20. K. Creath, "Phase measurement interferometry techniques," *Progress in Optics*, E. Wolf, ed., North Holland, Amsterdam, vol. XXVI, pp. 351-391, 1988.

21. J. T. Verdeyen, *Laser Electronics* (Prentice Hall, New Jersey, 1995) pp. 70-73.

22. P. Hariharan, B. F. Oreb, and T. Eiju, "Digital phase-shifting interferometry: a simple error-compensating phase calculation algorithm," *Applied Optics*, **26**(13), p. 2504, 1987.

23. D. C. Ghiglia and M. D. Pritt, *Two-Dimensional Phase Unwrapping: Theory, Algorithms, and Software*, John Wiley and Sons, New York, 1998.

24. V. V. Volkov and Y. Zhu, "Deterministic phase unwrapping in the presence of noise," *Optics Letters*, **28**(22), pp. 2156-2158, 2003.

25. M. A. Schofield and Y. Zhu, "Fast phase unwrapping algorithm for interferometric applications," *Optics Letters*, **28**(14), pp. 1194-1196, 2003.

26. A. Bosseboeuf and S. Petitgrand, "Characterization of the static and dynamic behavior of M(O)EMS by optical techniques: status and trends," *Journal of Micromechanics and Microengineering*, **13**, pp. S23-S33, 2003.

27. COMSOL Multiphysics, COMSOL Inc., http://www.comsol.com

28. W. N. Sharpe, S. B. Brown, G. C. Johnson, and W. G. Knauss, "Round robin tests of modulus and strength of polysilicon," *Materials Research Society Proceedings,* San Francisco, CA, vol. 518, pp. 57–65, 1998.

29. B. D. Jensen, M. P. de Boer, N. D. Masters, F. Bitsie, and D. A. La Van, "Interferometry of actuated microcantilevers to determine material properties and test structure nonidealities in MEMS," *Journal of Microelectromechanical Systems*, **10**(3), pp. 336-346, 2001.

30. O. Holmgren, K. Kokkonen, V. Kaajakari, A. Oja, and J. V. Knuuttila, "Direct Optical Measurement of the Q Values of RF-MEMS Resonators," *IEEE Ultrasonics Symposium*, pp. 2112-2115, 2005.

31. C. Orsulak, T. Coakley, M. Zecchino, "Characterizing AFM Cantilevers with Dynamic MEMS Measurement," Veeco Application Notes [Online]. Available: www.veeco.com/pdfs.php/116.

32. L. A. J. Davis, D. R. Billson, D. A. Hutchins, and R. A. Noble, "Visualizing acoustic displacements of capacitive micromachines transducers using an interferometric microscope," *Acoustic Research Letters Online*, **6**(2), pp. 75-79, 2005.

LABORATORY OPERATIONS

The Aerospace Corporation functions as an "architect-engineer" for national security programs, specializing in advanced military space systems. The Corporation's Laboratory Operations supports the effective and timely development and operation of national security systems through scientific research and the application of advanced technology. Vital to the success of the Corporation is the technical staff's wide-ranging expertise and its ability to stay abreast of new technological developments and program support issues associated with rapidly evolving space systems. Contributing capabilities are provided by these individual organizations:

Electronics and Photonics Laboratory: Microelectronics, VLSI reliability, failure analysis, solid-state device physics, compound semiconductors, radiation effects, infrared and CCD detector devices, data storage and display technologies; lasers and electro-optics, solid-state laser design, micro-optics, optical communications, and fiber-optic sensors; atomic frequency standards, applied laser spectroscopy, laser chemistry, atmospheric propagation and beam control, LIDAR/LADAR remote sensing; solar cell and array testing and evaluation, battery electrochemistry, battery testing and evaluation.

Space Materials Laboratory: Evaluation and characterizations of new materials and processing techniques: metals, alloys, ceramics, polymers, thin films, and composites; development of advanced deposition processes; nondestructive evaluation, component failure analysis and reliability; structural mechanics, fracture mechanics, and stress corrosion; analysis and evaluation of materials at cryogenic and elevated temperatures; launch vehicle fluid mechanics, heat transfer and flight dynamics; aerothermodynamics; chemical and electric propulsion; environmental chemistry; combustion processes; space environment effects on materials, hardening and vulnerability assessment; contamination, thermal and structural control; lubrication and surface phenomena. Microelectromechanical systems (MEMS) for space applications; laser micromachining; laser-surface physical and chemical interactions; micropropulsion; micro- and nanosatellite mission analysis; intelligent microinstruments for monitoring space and launch system environments.

Space Science Applications Laboratory: Magnetospheric, auroral and cosmic-ray physics, wave-particle interactions, magnetospheric plasma waves; atmospheric and ionospheric physics, density and composition of the upper atmosphere, remote sensing using atmospheric radiation; solar physics, infrared astronomy, infrared signature analysis; infrared surveillance, imaging and remote sensing; multispectral and hyperspectral sensor development; data analysis and algorithm development; applications of multispectral and hyperspectral imagery to defense, civil space, commercial, and environmental missions; effects of solar activity, magnetic storms and nuclear explosions on the Earth's atmosphere, ionosphere and magnetosphere; effects of electromagnetic and particulate radiations on space systems; space instrumentation, design, fabrication and test; environmental chemistry, trace detection; atmospheric chemical reactions, atmospheric optics, light scattering, state-specific chemical reactions, and radiative signatures of missile plumes.

THE AEROSPACE CORPORATION
2350 E. El Segundo Boulevard
El Segundo, California 90245-4691
U.S.A.